J. Electrochem. Sci. Eng. **14(6)** (2024) 803-822; http://dx.doi.org/10.5599/jese.2478

Open Access : : ISSN 1847-9286
www.jESE-online.org

Original scientific paper

Screen-printed electrode for electrochemical detection of sunitinib malate for therapeutic drug monitoring

Arun Warrier[1], Pooja Das Manjulabhai[1], Aiswarya Rajesh[1], Unnimaya Shanmughan[1], Varsha Vijayakumar[1], Jeethu Raveendran[2] and Dhanya Gangadharan[1,✉]

[1]*Department of Biotechnology, Sahrdaya College of Engineering & Technology, APJ Abdul Kalam Technological University Thiruvananthapuram, Kodakara, Thrissur, Kerala, India*
[2]*Department of Biomedical Engineering, Sahrdaya College of Engineering & Technology, APJ Abdul Kalam Technological University Thiruvananthapuram, Kodakara, Thrissur, Kerala, India*

Corresponding author: ✉*dhanyag@sahrdaya.ac.in, Tel.: +91-480-2726630*

Received: August 21, 2024; Accepted: November 28, 2024; Published: December 10, 2024

Abstract

Sunitinib is a targeted therapy for colorectal cancer, which needs a precise dosage due to potential severe side effects from overdose. Therapeutic drug monitoring is crucial for maintaining optimal drug levels in body fluids. Traditional anticancer drug dose evaluation methods such as high-pressure liquid chromatography, liquid chromatography with mass spectrophotometry, and immunoassays are cumbersome. This study explores the utilization of electrochemical sensors on indigenously developed screen-printed electrodes for sunitinib malate monitoring. Differential pulse voltammetry, cyclic voltammetry and chrono-amperometric studies were conducted in a conventional three-electrode system. An anodic peak current, indicative of sunitinib malate electrooxidation, was observed around +0.45 V vs. Ag/AgCl reference electrode in 0.1 M PB of pH 7.4. Sensitivity, the limit of detection and method detection limit were determined as 0.386 μA μM^{-1} cm^{-2}, 0.009 and 0.0108 μM, respectively. The response exhibited linearity (R^2 = 0.990) with sunitinib concentration ranging from 0.08 to 88 μM with good reproducibility. DPV studies on real samples yielded acceptable recovery values. Electrochemical sensors based on the screen-printed electrode present a promising approach for sunitinib monitoring, offering sensitivity, low limit of detection, and a wide linear range. Since the expected plasma concentration of sunitinib is much higher than the sensor detection range, it can be used for real sample analysis. Here developed methods could simplify and improve therapeutic drug monitoring in colorectal cancer treatment.

Keywords

Anticancer drug; electrooxidation; differential pulse voltammetry; real samples; electrochemical sensor

Introduction

Cancer is one of the major causes of mortality worldwide, yet its impact varies [1]. Some therapies now used to treat cancer include surgery, radiation, chemotherapy, and targeted therapy [2]. Chemotherapy, which uses specialised medications such as sunitinib, sorafenib, arsenic trioxide, asparaginase, dexamethasone, and dactinomycin, is the most effective of all of these therapeutic options [3,4]. The optimum therapeutic dosage for treating the condition is quite important. The high dosage of the drug shows toxic effects, whereas the low dose of the drug does not show any significant therapeutic effect [5]. Since real-life cancer patients are usually older, have comorbidities, and are on many medications, the pharmacokinetics of oral anticancer drugs are highly variable, particularly in terms of bioavailability [6,7]. Therapeutic drug monitoring (TDM) is used to determine the metabolite concentration in the blood or serum/plasma at a given time to see if drug concentrations are within therapeutic limits and either sub-therapeutic or dangerous for patients [8]. The quantitative analysis for TDM was performed by high-pressure liquid chromatography [HPLC], immunoassay and mass spectroscopy (MS) [9]. The major pitfalls of the current methodologies include high price, tedious and time-consuming procedures and a need for trained personnel for handling [10].

Electrochemical methods for effective TDM have been developed to provide a low-cost, easy-to-use, on-site analysis method for accessing the full potential of therapeutic drug monitoring and overcoming the limitations mentioned above [11,12]. This research focuses on a chemotherapeutic drug, sunitinib malate (STB), recommended for the treatment of gastrointestinal cancer or for patients who are intolerant to imatinib mesylate. STB is a multiple receptor tyrosine kinase inhibitor, which is considered effective in treating several tumours, including breast, lung and prostate cancers [10,11,13-15]. The capacity of STB to target several receptors results in a variety of side effects, including hand-foot syndrome, stomatitis, and other dermatologic toxicities. Hence, providing an optimal therapeutic dosage through therapeutic drug monitoring would benefit a patient undergoing chemotherapy [16].

In comparison to existing detection methods and electrochemical sensors for STB, our indigenously prepared screen-printed electrode sensor offers distinct advantages in terms of detection range and sensitivity. Traditional chromatographic methods such as high-performance liquid chromatography-tandem mass spectrometry (HPLC/MS/MS) and ultra-performance liquid chromatography-tandem mass spectrometry (UPLC/MS/MS) have demonstrated high sensitivity with rather low detection limits of 2-20 nM in serum samples [17-19]. However, these methods often require complex sample preparation and extensive instrumentation, limiting their applicability in rapid point-of-care settings.

In electrochemical detection, it has already been reported that polyacrylonitrile nanofibers/$Ni_{0.5}Zn_{0.5}Fe_2O_4$ nanoparticles can be used as novel sensor material for detecting STB [3]. Vercelli *et al*. reported the use of Nafion-modified glassy carbon electrode (GCE) to determine the concentrations of STB [14]. The authors focused on the redox properties of STB and irinotecan molecules using cyclic voltammetry and differential pulse voltammetry techniques. This research revealed distinct electrochemical signatures for each drug, providing insights into their electron transfer mechanisms, which shows the importance of electrochemical detection for STB. Zhang and Li [20] developed an electrochemical sensor designed to detect the anticancer drug STB using a nanocomposite of metal-organic frameworks (MOFs) and carbon nanotubes (CNTs) on a GCE, which demonstrates a linear response over the concentration range from 0.02 to 30 µM. Additionally, it exhibited a notable detection limit of 5 nM, highlighting its potential for highly sensitive and selective pharmaceutical analysis and monitoring of therapeutic drug levels in clinical settings.

These previously reported works use highly expensive modifications of GCE for the quantitative and qualitative analysis of STB. Our work introduces cost-effective, fully disposable, indigenously prepared screen-printed electrodes. The electrochemical studies were carried out using differential pulse voltammetry (DPV), cyclic voltammetry (CV) and chrono-amperometry techniques on the screen-printed electrodes. The linearity of the drug response to STB concentrations was studied for each electrochemical technique. The repeatability of the procedure was confirmed, and the electrode sensitivity was further evaluated. The effect of common interfering molecules such as glucose, sucrose, ascorbic acid, uric acid and dopamine were also examined. The accuracy of the sensor was studied in body fluids, including blood serum and urine samples. It was found suitable for analysing sunitinib malate in urine, blood, and tablet formulations with comparable sensitivity to advanced electrochemical methods like fluorescence-based detection using nitrogen-doped graphene quantum dots (N-GQDs) [13]. This demonstrates the potential of our screen-printed electrodes (SPE) for sensitive and selective detection of sunitinib malate across diverse sample matrices, highlighting its utility in biomedical research and clinical diagnostics.

Experimental

Reagents

The pharmaceutical grade STB was procured as a gift from a pharmaceutical company and directly used. Deionized water (DI water) was obtained from STERLABS and used to prepare the reagents and supporting electrolytes. A stock solution of 4.0 mmol L^{-1} STB was prepared by dissolving the accurate mass of the drug in an appropriate volume of DI water and kept in the dark in a refrigerator. The working solutions for the voltammetric investigations were prepared by diluting the stock solution with the supporting electrolyte (0.1 M phosphate buffer) daily. 1 mol L^{-1} phosphate buffer (pH 7.4) was prepared using sodium hydrogen phosphate (Na_2HPO_4, Nice Chemical (P) Ltd, Kerala) and potassium dihydrogen phosphate (KH_2PO_4, Nice Chemical (P) Ltd, Kerala).

Potassium ferricyanide ($K_3Fe(CN)_6$, Merck, Germany), 5 mmol L^{-1} in potassium chloride (KCl, Nice Chemical (P) Ltd, Kerala), 0.1 mol L^{-1} was prepared as 100 ml of solution.

All electrochemical studies were carried out on screen-printed electrodes (SPE) in 0.1 M phosphate buffer (PB) of pH 7.4. Conductive inks of carbon (Code No: 050, Sun Chemical C2030519P4, Siltech Corporation Inc., Bangalore), silver (Code No: 060, Siltech Corporation Inc., Bangalore), and Ag/AgCl paste (CAS No: 7783-90-06, Product Code: NCZ-SPI-104, Nanochemazone, Chemazone Inc., Canada) were used for the fabrication of screen-printed electrodes. ADSUNIB™ capsules (ADLEY Formulations, Himachal Pradesh, India) were purchased from Amala Institute of Medical Science, Private Medical College, Thrissur was labelled to contain 12.5 mg STB per tablet.

Apparatus

A three-electrode system consisting of a glassy carbon working electrode (GCE; diameter = 2 mm), a platinum wire auxiliary electrode and an Ag/AgCl (KCl, 3 mol L^{-1}) reference electrode was procured from PSP Instruments, Mumbai.

Indigenously prepared screen-printed electrodes were characterized by field emission scanning electron microscopy (FE-SEM) and X-ray diffraction (XRD). FE-SEM images were obtained with Thermo Fisher FEI QUANTA 250 FEG, USA. XRD analysis was done on an Aeris Research Benchtop X-Ray Diffractometer (Malvern Panalytical, UK). In the study, electrochemical measurements were made using the cyclic voltammetry (CV) and differential pulse voltammetry (DPV) methods on the DY2300 series bi-potentiostat (Germany) device, using DY2300EN software. For the analytical

application, the following parameters were employed: pulse amplitude 50 mV; frequency 90 Hz, potential step 10 mV (DPV), and the scan rate 50 mV s^{-1} (CV). Electrochemical impedance spectroscopy (EIS) measurements were taken using the Electrochemical Workstation Model: CHI6005E, IIT Palakkad. Amplitude, frequency range and measuring potential used to perform EIS were 0.005 V, 100 kHz to 0.05 Hz and 0.2 V *vs*. Ag/AgCl, respectively. In some stages of the study, a microprocessor-based pH meter (Esico, Model 1010, India) and precision balance (Infra Instruments Pvt Ltd, Chennai) were used for pH and weight measurements, respectively.

Fabrication of screen-printed electrodes

Two sets of screen-printed electrodes with a conventional three-electrode system (working, reference, and counter electrodes) were screen-printed on poly(ethylene terephthalate) (PET) sheets. Designs used for the screen-printing technique are given in the *Supplementary material* (Figure S1). PET sheets were preheated at 100 °C for one hour. Silver ink was screen printed as the base layer on PET sheets, and the sheets were air-dried for one hour. The carbon layer was subsequently printed. This layer was dried at 60 °C for one hour. Ag/AgCl ink was printed on the tip of the reference carbon track and dried at 60 °C for one hour. The electrodes were named screen-printed electrodes (SPE). The second set of electrodes was prepared without a silver layer, and all the procedures remained the same. These electrodes were named as screen printed carbon electrodes (SPCE). The developed electrodes have a geometric area of 3.14 mm^2 (r = 1 mm).

Electrochemical measurements

Electrochemical studies of STB were performed using CV, chrono-amperometry and DPV techniques in 0.1 M PB of pH 7.4. CV studies were conducted within the potential window of 0 to 0.7 V *vs*. Ag/AgCl with a scan rate of 50 mV/s. From the peak potential inference from CV, chronoamperometric studies were performed at a potential of 0.55 V for 20 s. Sensitivity, linearity, interference, and real sample studies were performed with DPV in a potential window of 0 to 0.8 V. All current values reported in this study were obtained after subtracting the background capacitive current, ensuring that the oxidative response of the analyte is accurately reflected.

The electrochemical behaviour of common interfering molecules like glucose, sucrose, maltose, ascorbic acid, uric acid, urea, dopamine, and sodium, potassium, magnesium, and calcium salts was studied. Blood and urine samples from healthy volunteers were collected. Blood was allowed to clot completely for two hours at room temperature, and serum was extracted by centrifuging the samples for 30 minutes at 5000 rpm. The separated serum and urine samples were characterized using DPV by spiking 100 µL of the samples into the buffer.

Preparation of pharmaceutical samples

STB tablets, purchased as ADSUNIB™ (12.5 mg), were ground into a uniform powder before electroanalysis. The weighed STB power was dissolved in dimethylformamide (DMF) and the solution was ultrasonically processed for 15 min. Filtration was used to take the undissolved excipients out of the solution. These tablet solutions were used to validate the sensor using the DPV technique.

Results and discussion

Electrochemical optimization

The electrochemical active area plays an important role, as it helps to know the area where the reaction takes place. For some carbon electrodes, it is usually lower than the geometric area [21].

To determine the electrochemically active area, the developed sensor was examined with varying potential scan rates for 5 mM $[Fe(CN)_6]^{3-/4-}$ + 0.1 M KCl. The cyclic voltammograms obtained for varying scan rates from 5 mV s^{-1} to 1 V s^{-1} are shown in Figure 1a, while the associated anodic and cathodic peak currents obtained were plotted against scan rates in Figure 1b. The linear relationship between the peak current and the square root of the scan rate confirms that the charge transfer of $[Fe(CN)_6]^{3-/4-}$ is a diffusion-controlled reaction. Furthermore, the electrochemically active area can be determined using the Randles-Ševčik relation [34]:

$$I_p = 2.69\times10^5\, n^{3/2} A D^{1/2} C v^{1/2} \quad (1)$$

where C is the concentration of $[Fe(CN)_6]^{3-/4-}$, I_p / µA is peak current, D is diffusion coefficient (7.6×10^{-6} cm^2 s^{-1}), n = 1 is the number of electrons, v / mV s^{-1} is scan rate and A / cm^2 is electrode surface area. Comparing Equation (1) with the linear regression equation obtained for anodic peak current and square root scan rate, I_{pa} = 3.13 $v^{1/2}$ - 7.22 (R^2 = 0.988), will give the effective electrochemical active area. Using recorded signals and Equation (1), the active surface area of SPE was found to be 0.844 cm^2.

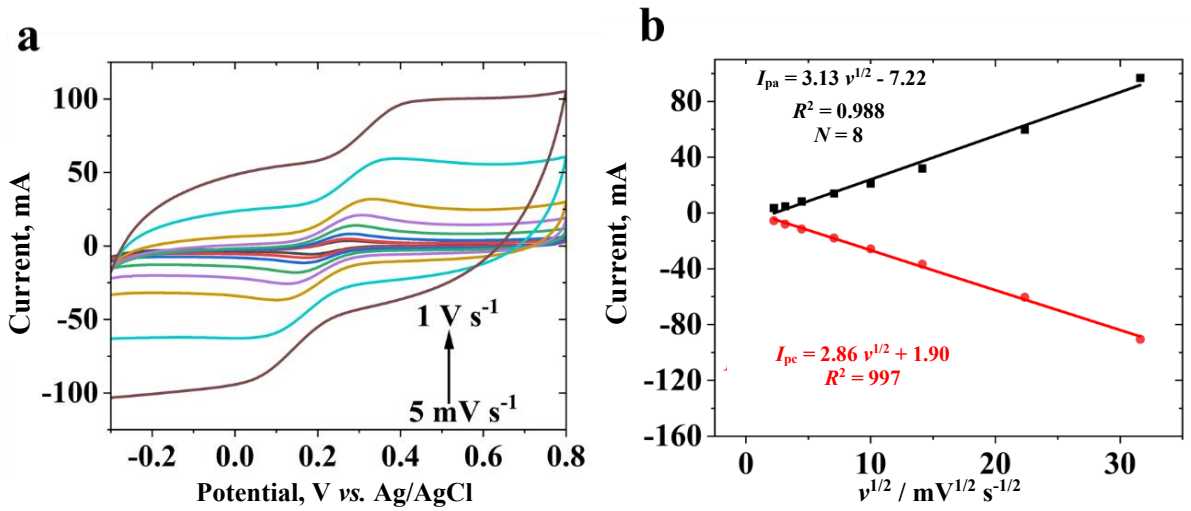

Figure 1. *Cyclic voltammograms of SPE in 0.1 M KCl with 5 mM $[Fe(CN)_6]^{3-/4-}$ at various scan rates (a), plots of anodic and cathodic peak currents (I_{pa} and I_{pc}) versus square root of scan rate (b)*

Electrochemical impedance spectroscopy measurements

The electrochemical impedance spectroscopy (EIS) experiments were performed using the redox probe, $[Fe(CN)_6]^{3-/4-}$, to investigate the electrochemical behaviour of developed electrodes. This gave further insight into the electrochemical properties and performance of the developed electrodes and, was discussed in more details in the *Supplementary material*. The relevant parameter used for the study is charge transfer resistance (R_{ct}), *i.e.,* the resistance of the electron transfer of $[Fe(CN)_6]^{3-/4-}$ between the electrode and the solution. The results of Nyquist plots for SPE in 0.1 mol L^{-1} KCl containing 5 mmol L^{-1} $[Fe(CN)_6]^{3-/4-}$, obtained over the frequency range of 100 kHz to 0.05 Hz, are shown in Figure S2. In conclusion, the electrode demonstrated excellent performance with low charge transfer resistance, indicating efficient electrochemical reaction and good electrode conductivity. The transition to diffusion-limited behaviour at lower frequencies further suggested that the electrode maintains fast kinetics.

Choice of electrode

Electrooxidation of STB was studied on three sets of electrodes, namely, glassy carbon electrode (GCE), SPCE, and SPE. A comparative study of a random concentration of STB (56 µM) on GCE, SPCE,

and SPE using DPV technique was carried out with 56 µM STB in 0.1 M PB of pH 7.4. It is shown in Figure 2 that all electrodes showed the anodic peak, indicating electrochemical oxidation of STB on each electrode. Dotted lines denote background currents obtained without STB for each electrode. GCE, SPCE, and SPE exhibited a slight increase in oxidation potential at 0.45 V, 0.48 V, and 0.45 V, respectively. On comparing the anodic peak currents values, GCE showed the lowest peak current (7.51 µA), than SPCE (14.412 µA), while the highest oxidation current was observed for SPE with I_{pa} of 21.967 µA. According to Figure 2, SPE showed the highest anodic current and the most favourable potential for the oxidation of STB. The presence of the silver layer beneath the carbon layer reduces the charge transfer resistance (R_{ct}) in the sensor, leading to a shift in the peak potential toward a more favourable oxidation potential. Hence, SPE was used for all further studies.

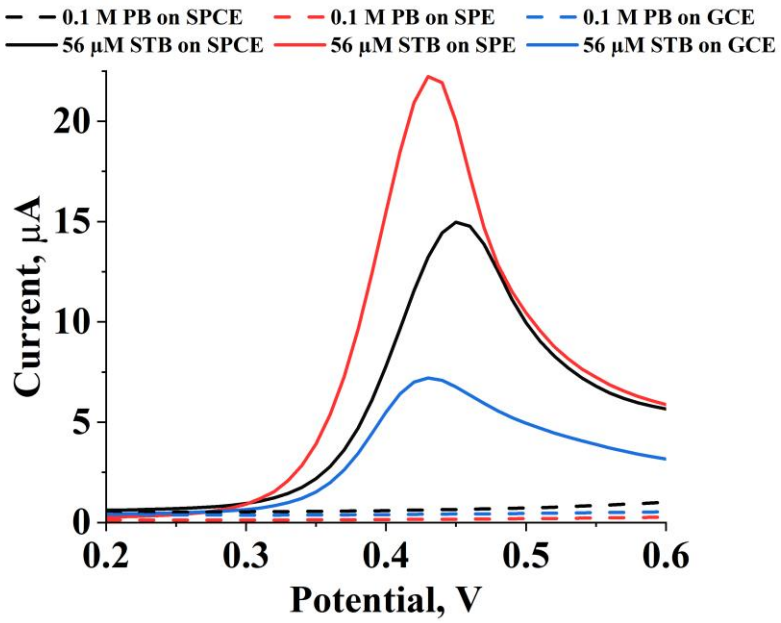

Figure 2. *Differential pulse voltammograms of 56 µM STB in 0.1 M PB of pH 7.4 on SPCE (black line), SPE (red line) and GCE (blue line)*

Morphological and elemental characterization of screen-printed electrodes

The surface morphology of SPE was examined with FE-SEM. Figures 3a and b show the microscopic images at different magnifications. Microscopic images showed the uniform distribution of granular carbon nanoparticles of approximately 40 nm diameter on the sensor surface. EDAX spectrum (Figure 3c) confirmed that the exposed surface is mainly formed of carbon (100 % carbon with Ag traces). Figure 3d shows the XRD spectrum, showing peaks at 2θ values corresponding to silver (*e.g.*, around 38.2, 46.18 and 64.5°) [23] and graphite (*e.g.* around 26.5°) [24,25]. In addition, the peaks at 42.91 and 44.94° are connected to the carbon in-plane (100) and (101) reflections, respectively, while the peak at 65.74° is connected to the XRD of carbon from (004) reflection [24,25]. These peaks correspond to distinct crystallographic planes characteristic of the materials present in the electrode composition. The peak observed at $2\theta \approx$ 26.5° is attributed to the (002) plane of graphite. The XRD pattern peaks at 2θ= 26.34, 46.18 and 53.48° correspond to carbon nanotubes structural peak, which justifies the SEM result of carbon being in its nano-size [26]. The observed peak positions for graphite [26,27] and silver [25,28] in our XRD analysis align well with previous studies on similar electrode materials. This indicates the presence of graphitic carbon within the electrode material. This large and intense peak signifies that the electrode material is predominantly composed of graphitic carbon. Graphitic carbon is known for its high electrical conductivity and stability, which are favourable properties for

electrode applications [23,28]. Peaks at $2\theta \approx$ 38.2, 46.18 and 64.5° correspond to the (111), (200), and (220) planes of silver, respectively, indicating the silver nanoparticles are fcc (face centred cubic) and crystalline (JCPDS file no. 84-0713 and 04-0783). These peaks confirm the presence of crystalline silver nanoparticles or silver phases in the electrode structure. The relatively smaller intensities of these silver peaks suggest that it is present in lower abundance compared to graphite in the screen-printed electrodes. The presence of silver is crucial as it can enhance the conductivity and catalytic properties of the electrode material, particularly in electrochemical applications [23,28]. The presence of graphitic carbon suggests a stable conductive matrix essential for efficient charge transfer during electrochemical processes. Moreover, the presence of silver nanoparticles enhances the electrode's catalytic activity, making it suitable for applications requiring high performance in electrochemical sensing [29,30]. The peak at 26.5° at the 002 plane confirmed that the conductive ink used in SPE is graphite and in primitive hexagonal form (JCPDS database- 41-1487) [31].

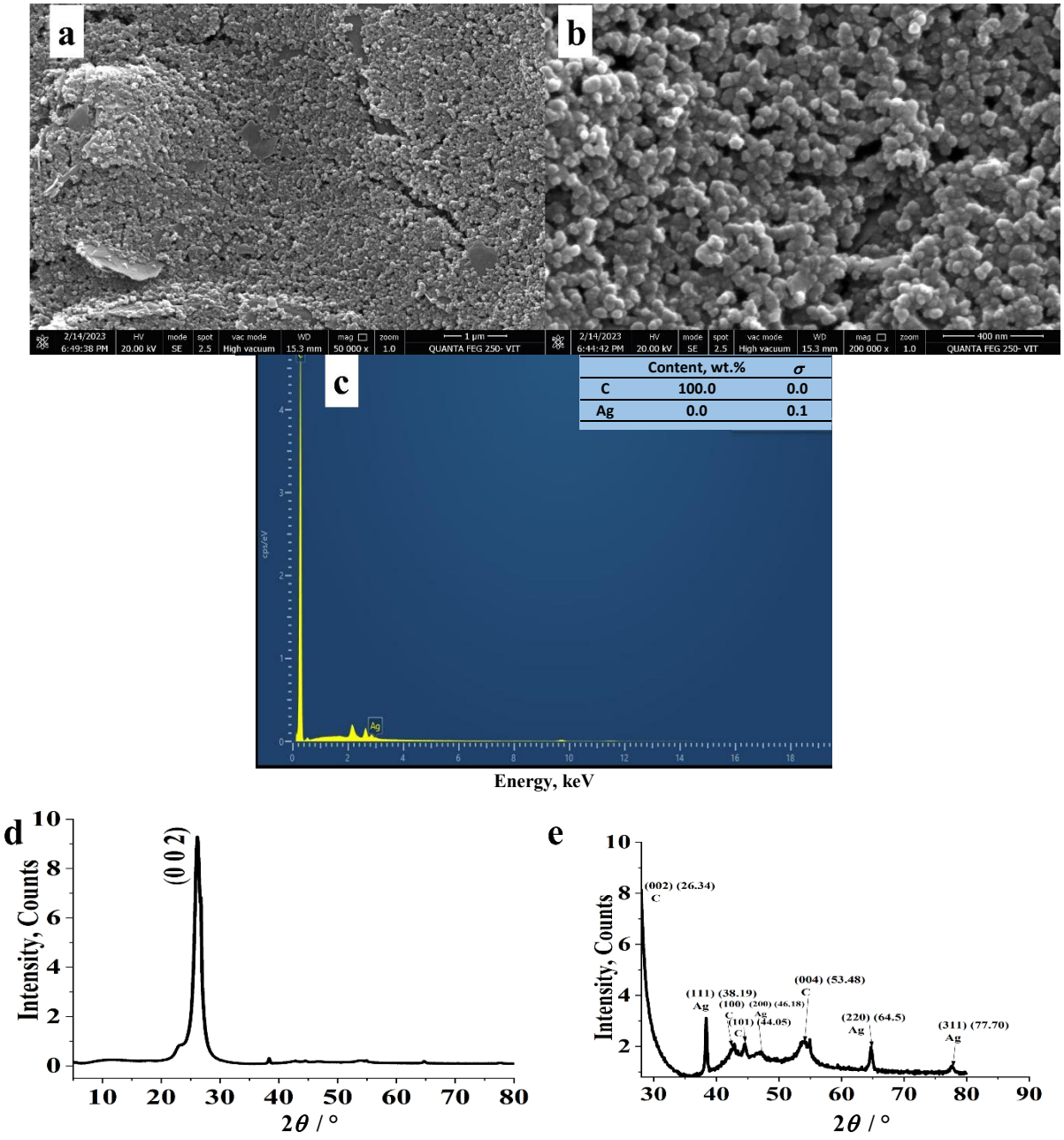

***Figure 3**. FE-SEM images at different magnifications (a,b), EDAX spectrum (c) and XRD spectrum (d) of SPE and of lower peaks in the XRD spectrum (e)*

Effect of type and concentration of supporting electrolyte

Electrochemical oxidation of 30 µM STB on SPE was studied in phosphate buffer (PB) and Trizma buffer (TB) as supporting electrolytes (0.1 M, pH 7.4). The obtained DPV responses are shown in Figure 4a. The responses show that the oxidation of STB is more favourable in PB, with a peak anodic potential at 0.45 V. The peak anodic potential for TB was found to be at 0.6 V. The peak anodic currents for STB in PB and TB were 11.07 and 4.82 µA, respectively. Further effects of the supporting electrolyte concentration were studied in 0.05 M, 0.1 M and 0.2 M PB. The DPV analysis for 30 µM STB in 0.1 M PB, similar to the physiological ionic concentration in body fluids, showed the highest current of 11.07 µA at the favourable E_{pa} of 0.45 V (Figure 4b).

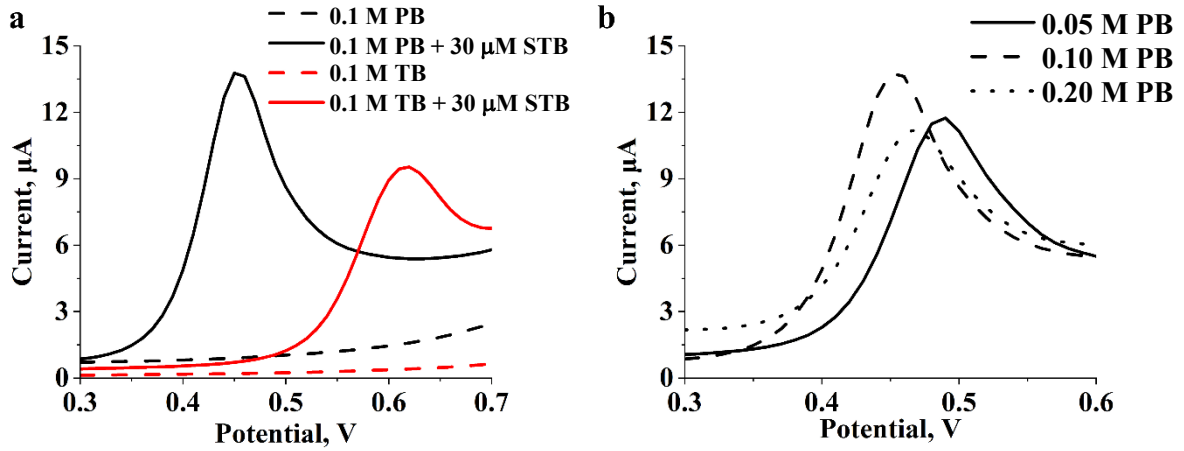

Figure 4. *Differential pulse voltammograms of SPE for 30 µM STB in 0.1 M trizma and phosphate buffers, pH 7.4 (a) and 0.05, 0.1 and 0.2 M phosphate buffer, pH 7.4 (b)*

Henceforth, all further investigations of STB were carried out in the optimal supporting electrolyte of 0.1 M PB (pH 7.4).

Electrochemical behaviour of sunitinib malate

The electrochemical fate of STB at redox scans was analysed using CV within a potential window of 0 to 0.7 V *vs*. Ag/AgCl with a scan rate of 50 mV s^{-1}. Figures 5a and 5b show CVs recorded with different concentrations of STB, ranging from 0.8 to 5.6 µM and 8 to 88 µM, respectively. Two anodic peaks at 0.2 V and 0.45 V were observed in each cyclic voltammogram. This conductive carbon paste serves as the base material for the electrode, facilitating electron transfer during the electrochemical reactions, and it is responsible for the oxidation peak observed around 0.2 V. While the one at 0.45 V is attributed to the oxidation of STB in a 0.1 M PB solution [17,32,33]. The absence of a cathodic peak indicates that the electrochemical reaction of the drug is irreversible. The oxidation potential is slightly shifted toward a more positive potential with an increase in concentrations of STB. A linear relationship is observed between I_{pa} and the concentration of STB. Figure 5c shows the calibration plot, *i.e.,* the dependence of peak oxidation current on STB concentration (0.8 to 88 µM), while the inset of Figure 5c shows the linear regression fitting of STB at lower concentrations (0.8-5.6 µM). The linear regression fitting equation of STB in the concentration range 0.8 to 88 µM, was found to be $I_{pa} = 0.123\ C + 2.31$ with a regression coefficient of 0.977.

Chronoamperometry studies were performed at the constant oxidation potential of 0.55 V, and the obtained curves are shown in Figure 6. The results clearly show that the oxidative reaction of STB produces an output current that is linearly increasing with the STB concentration. $I_{pa} = 0.053\ C + 0.367$ ($R^2 = 0.975$) is the linear regression equation obtained from chronoamperometry experiments.

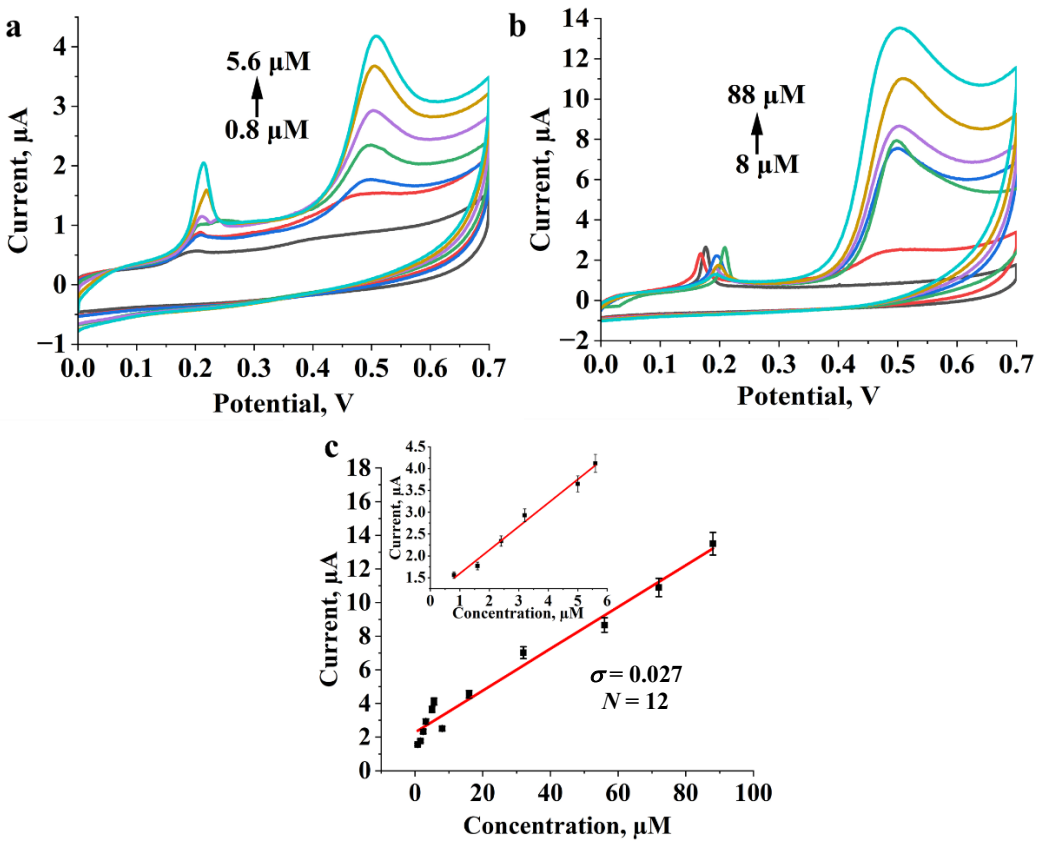

Figure 5. *Cyclic voltammograms (0.5 mV/s) of SPE in 0.1 M PB, pH 7.4 with different concentrations of STB 0.8 to 5.6 µM (a) and 8 to 88 µM (b); linear regression fitting of peak current versus concentration (0.8 to 88 µM) (c), inset: linear regression fitting for lower concentration of STB (0.8 to 5.6 µM)*

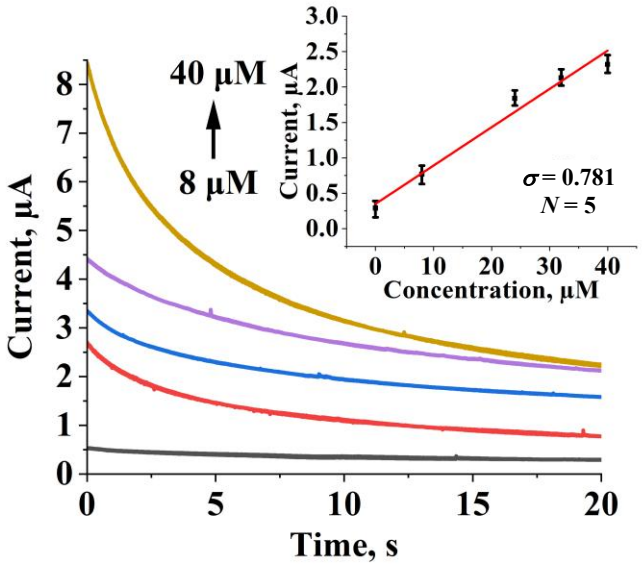

Figure 6*. Chrono-amperometric i-t curves obtained for SPE in 0.1M PB, pH 7.4 with different concentrations of STB (8 to 40 µM); inset: linear regression fitting of peak current versus STB concentration at t = 20 s*

A more resolved oxidation peak of STB was obtained by the DPV technique. Electrochemical responses for different concentrations of STB, ranging from 0.08 to 0.64 µM, 0.8 to 8.8 µM and 8 to 88 µM, were recorded on individual electrodes and shown in Figures 7a-c. A linear increase in the anodic current with an increase in STB concentration is generally observed for all DPVs. The linear regression equation obtained for the indigenously prepared SPE in the total STB concentration range from 0.08 to 88 µM was found to be I_{pa} = 0.326 C + 0.161 (R^2 = 0.993), with electrode sensitivity of

0.386 µA μM^{-1} cm^{-2}. Target total plasma concentrations of STB plus the active metabolite (N-desethyl sunitinib) are estimated from pharmacokinetic studies to be in the range of 50 to 100 ng ml^{-1} (97 to 194 nM) [34]. The expected plasma concentration of sunitinib is much higher than the sensor detection range, so the developed sensor can be used for real sample analysis.

The oxidation potential shift to the right was also observed with the increase in the concentration of STB, which may be attributed to the weak adsorption of STB onto the surface of SPE [35]. The limit of detection (LOD) and limit of quantification (LOQ) were obtained as 0.009 and 0.030 µM, respectively, using Equations (2) and (3):

$$LOD = 3S_b/m \quad (2)$$

$$LOQ = 10S_b/m \quad (3)$$

S_b (9.83×10^{-4}) is the standard deviation of anodic current corresponding to six blanks at 0.45 *V* and *m* is the slope from the I_{pa} versus concentration plot.

The method detection limit (MDL) is typically determined by analysing a sample with known low concentrations of the target analyte and calculating using Equation (4):

$$MDL = \frac{ts}{\text{Slope}} \quad (4)$$

where *t* is the Student's *t*-value for a desired confidence level (three replicates), *s* is the standard deviation of the blank measurements, and Slope is derived from the calibration curve. We calculated the MDL using the linearity values derived from our concentration measurements in nM. The MDL provides a more accurate representation of the lowest concentration that can be reliably detected using our electrochemical method. The calculated MDL is approximately 0.0108 µM.

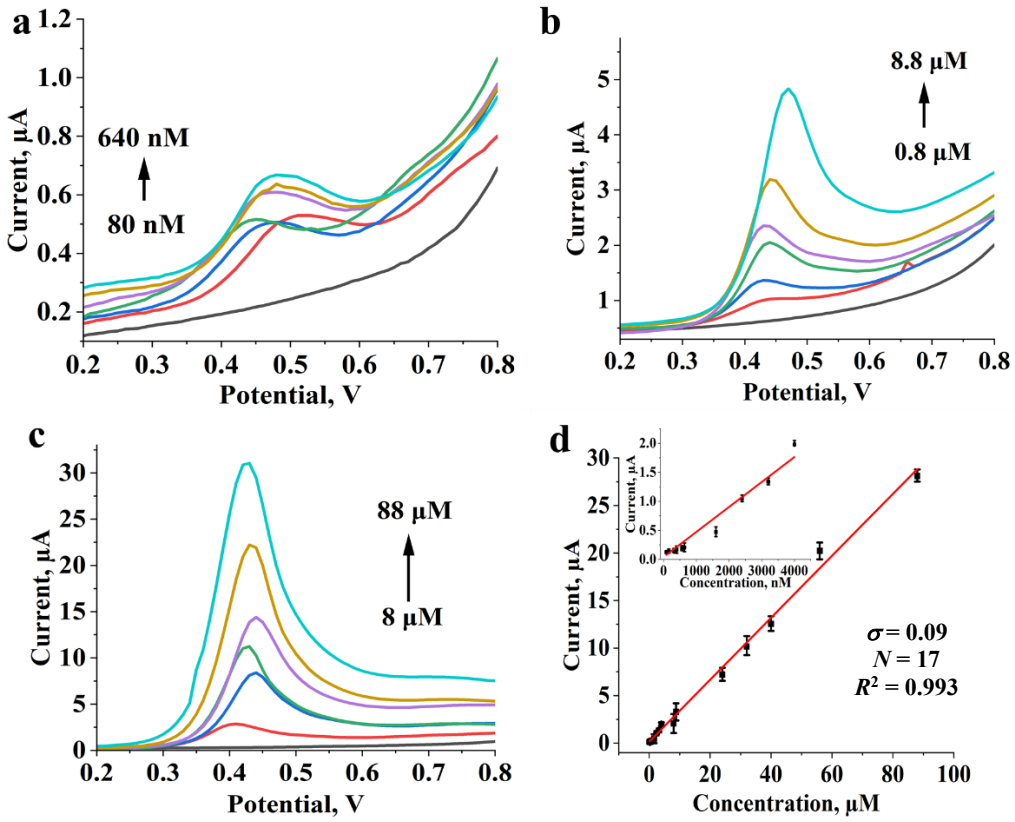

Figure 7. *Differential pulse voltammograms of SPE in 0.1 M PB, pH 7.4 with a - 0.08 to 0.64 (a), 0.8 to 8.8 (b) and 8 to 88 µM STB (c); calibration plot of STB peak current versus concentration for the total concentration from 0.08 to 88 µM (d), inset: linear regression plot for lower concentrations of STB (0.08 to 4 µM)*

Effect of scan rate

The relationship between anodic peak current and scan rate was analysed to identify the oxidation mechanism. CVs were recorded with 40 µM STB in 0.1 M PB at pH 7.4 for different scan rates, ranging from 1 to 200 mV s^{-1} (Figure 8a). The peak currents increased with the increase in scan rate. Figures 8b and 8c show plots of anodic peak current versus scan rate and the square root of the scan rate, respectively.

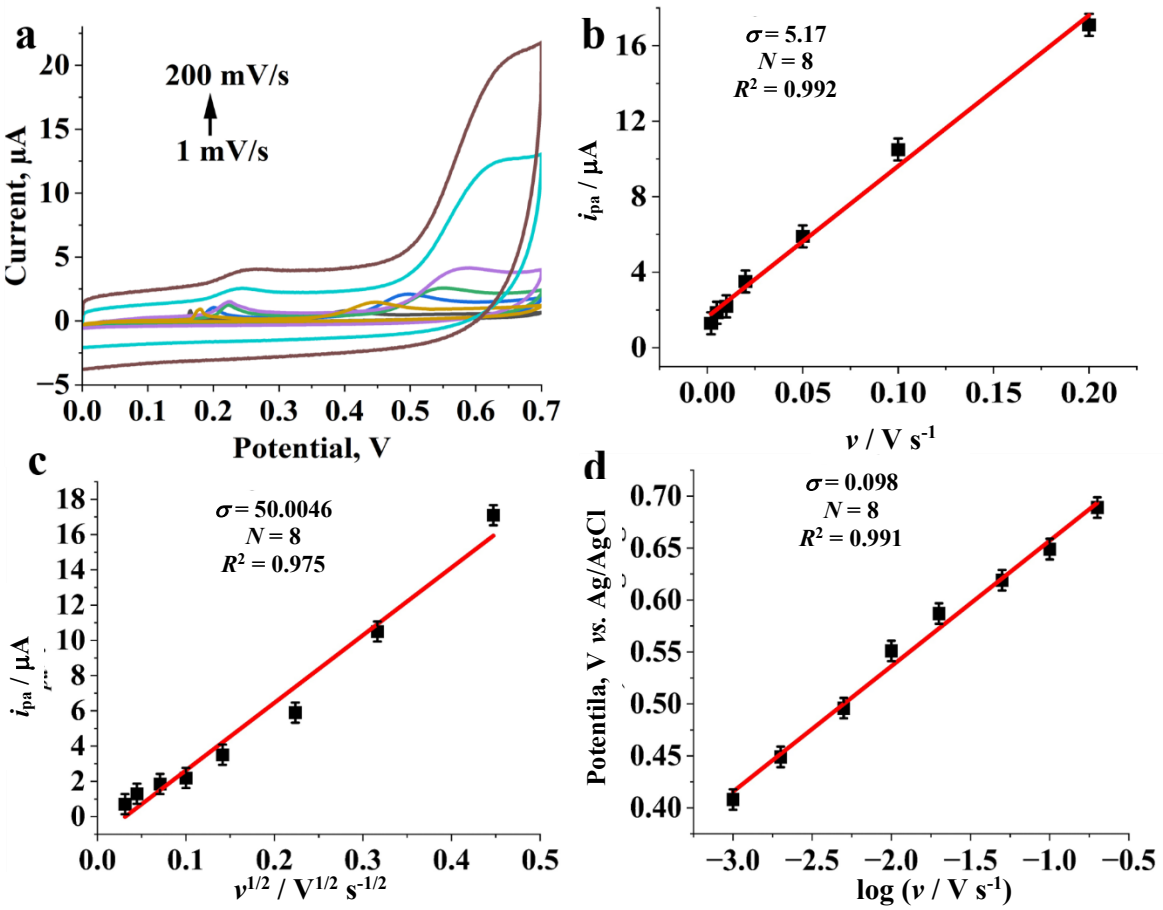

Figure 8. *Cyclic voltammograms of SPE in 0.1 M PB, pH 7.4 and 40 µM STB at various scan (a); plots of anodic peak current versus scan rate (b) and square root of scan rate (c); plot of anodic peak potential versus log of scan rate (d)*

The regression coefficient for the plot in Figure 8b (R^2 = 0.992) was found to be greater than that for the plot in Figure 8c. The excellent linear relationship between peak current and scan rate shown in Figure 8b confirmed that the oxidation of STB is a Nernstian adsorption-controlled phenomenon, and the reaction obeys Equation (5) [44,47-49]:

$$I_{pa} = \frac{n^2F^2}{4RT} \nu A \Gamma_0 \quad (5)$$

where I_{pa} is the anodic peak current, n is the number of electrons taking part in the reaction, F is the Faraday constant (96485 C mol^{-1}), ν / V s^{-1} is the scan rate, Γ_0 is the amount of surface coverage in mol cm^{-2} and A is the area of the electrode that was calculated to be 0.844 cm^2, R is the universal gas constant and T is temperature.

The number of electrons involved in the oxidation reaction of the drug was calculated using the Laviron Equation (6) [36]:

$$E_{pa} = E_0 + \frac{2.303RT}{(1-\alpha)nF}\log \nu \quad (6)$$

where E_{pa} is anodic peak potential, E_0 / V represents the formal potential, R is the universal gas constant with a value of 8.314 J K^{-1} mol^{-1}, T = 298 K is the working temperature, n is the number of electrons undergoing reaction, F is Faraday's constant with a value of 96485 C mol^{-1}, ν is the scan rate and α is the transfer coefficient, which value is 0.5.

E_{pa} was calculated using the linear regression equation of linear plot representing peak potential *versus* scan rate, which was determined ba Equation (7):

E_{pa} = 0.121 log ν + 0.778, R^2 = 0.992 (7)

Equating the slopes of Equations (6) and (7) shows that 0.98 electrons were used in the oxidation reaction. This clearly shows that the electrooxidation of STB proceeds with the release of one electron in the presence of 0.1 M PB of pH 7.4 at 0.45 V. Using Equation (5), with n = 1 and A = 0.844 cm^2, the amount of surface coverage (Γ_0) was calculated to be 32 nmol cm^{-2}.

Interference studies

DPV was performed to analyse the selective recognition ability of the sensor for the detection of STB in the presence of common oxidising biomolecules found in real samples, including glucose (8.93 mM), sucrose (8.93 mM), maltose (8.93 mM), ascorbic acid (0.14 mM), uric acid (0.5 mM), urea (1.31 mM), dopamine (2 µM), and salts of sodium (0.5 mM), potassium (0.5 mM), magnesium (0.5 mM) and calcium (0.5 mM) (Figure 9a).

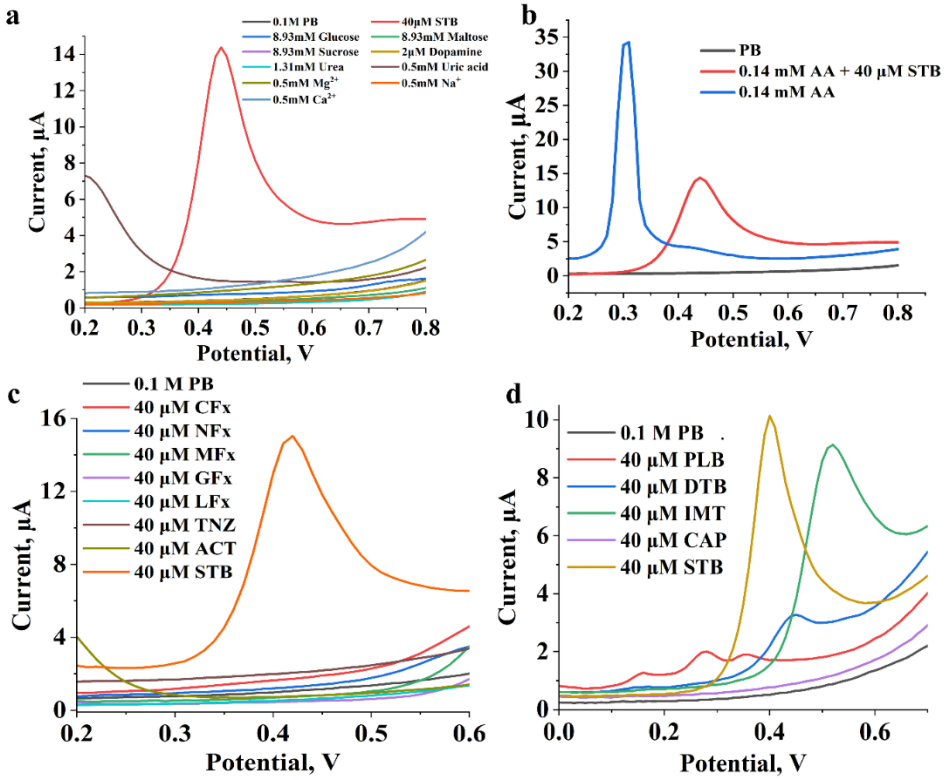

Figure 9. *Differential pulse voltammograms of SPE in the presence of biomolecules and common salts (a), ascorbic acid (b), fluoroquinolones (c) and similar class of drugs (d)*

The SPE responses obtained for the same concentrations (40 µM) of ciprofloxacin (CFx), norfloxacin (NFx), moxifloxacin (MFx), gatifloxacin (GFx), levofloxacin (LFx), tinidazole (TNZ) and acetaminophen (ACT) are shown in Figure 9c. The absence of oxidation peak at the requisite potential

of STB oxidation confirmed the selective detection of STB in 0.1 M PB on SPE. The selectivity of the sensor in the presence of similar drugs was also analysed. Figure 9b represents the voltammograms obtained when ascorbic acid was tested for its interference with STB; a more detailed study of this compound is shown in *Supplementary Material*, Figure S3. Figure 9d represents the voltammogram that was produced at the identical concentrations (40 μM) of dasatinib (DTB), palbociclib (PLB), imatinib (IMT) and capecitabine (CAP). All the molecules except CAP exhibited notable oxidation peaks in the applied potential range. However, the co-administration of these antineoplastic drugs is not practised in the current chemotherapy regimens reported [34,37,38]. Patients who are imatinib-resistant, or when imatinib fails to treat gastrointestinal stromal cancer (GIST), are administered by sunitinib [39,40]. Patients with metastatic renal cell cancer often receive sunitinib as the first line of treatment [37]. Therefore, this will not impact on our goal of developing an SPE sensor for the TDM of sunitinib in biological samples.

Contrary to Figures 9a and 9c, where different biomolecules and common ions do not show any characteristic peak in the recorded DPVs, Figure 9b shows some effects in the presence of ascorbic acid (AA). The DPV response for ascorbic acid showed an oxidation potential of 0.31 V, which is lower than the oxidation potential of STB (0.45 V). The effects of AA on the STB oxidation peak at SPE in 0.1 M PB were studied in more details by performing DPVs at the constant AA concentration (80 μM) and varying STB concentration (12, 14 and 36 μM), as well at the constant STB concentration (0.537 μM) (plasma concentration) and varying AA concentration (40, 80 and 100 μM). The resulting DPVs are shown in Figure S3(A) and (B) of the *Supplementary material*, suggesting that AA does not influence STB oxidation.

Real sample analysis

Real samples usually contain a variety of species that readily adsorb onto surfaces. The recovery percentage of the suggested sensors often decreases dramatically due to such non-specific adsorption. So, we performed recovery studies of the analyte in serum and urine samples to assess the performance of the proposed sensor. It was studied extensively. The good recovery values obtained for STB in real samples indicate that even changing the matrix did not induce a mass change in the diffusion flux of STB towards the sensor.

The blood serum and urine samples were analysed using the DPV technique in 0.1 M PB of pH 7.4. The matrix impact was investigated in the presence of 5 μL serum and urine samples in 0.1 M PB in a detailed manner, and results are presented in Figure S4 of the *Supplementary material*. The absence of anodic Faradaic currents indicated no oxidation in the requisite potential window for the serum or urine sample. The percentage of recovery of the sensor was studied by spiking known concentrations (5, 8, and 11 μM) of STB into the real samples. Table 1 shows the recoveries obtained in the real samples. The recovery of STB in blood serum samples was found to be 104.98 and 103.32 %, respectively. Similarly, 94.2 and 97.81 % recovery were found in urine samples and 97.97 % recovery for the ADSUNIB tablet. Many aspects of pharmacokinetic models cannot be derived from the proposed sensor. However, our sensor may be used to monitor medication concentrations in the blood *in vitro*, revealing distinct variations in [41,42] with respect to circulation that could significantly impact therapeutic efficacy and safety.

The standard addition approach has been employed to analyse drugs quantitatively. Measuring the DPV responses of pharmaceutical samples with STB added at a specified concentration was used in the spike and recovery tests. All pharmaceutical product solutions underwent three additions using STB standard solutions. The obtained results are shown in Table 1.

***Table 1**. Recovery study of STB in serum, urine samples and tablets*

Sample		Concentration, µM		Recovery, %
		Spiked	Recovered	
Serum	Sample 1	12	12.77	106.41
		24	24.31	101.30
		36	38.62	107.28
	Sample 2	12	12.38	102.92
		24	24.07	100.30
		36	38.43	106.75
Urine	Sample 1	0.537	0.48	89.57
		5	4.56	91.2
		8	7.82	97.75
		11	10.81	98.27
	Sample 2	0.537	0.50	92.55
		5	5.03	100.6
		8	8.1	101.25
		11	10.65	96.82
Tablet		12.15	10.92	89.92
		24.3	23.89	98.34
		36.45	39.81	109.24

Reproducibility and stability

Reproducibility was examined by detecting a triplicate set of STB samples. The reaction of STB in 0.1 M PB on fifteen distinct electrodes was investigated using DPV and results are shown in Figure S5(a) of the Supplementary material. The developed sensor exhibited a relative standard deviation of 3.5 %. The fabricated electrodes were kept at room temperature in an airtight, sealed condition. As stability was tested on different electrodes of the same batch for 30 days, no cleaning procedures were required. Every five days, responses for 40 µM STB in 0.1 M PB were estimated on different electrodes for 30 days. Results shown in Figure S5(b) of the Supplementary material indicate a drop in the response by 8.6 % towards the end of the month. The investigation showed that the lab-prepared SPE offers great reproducibility and stability when stored in a sealed condition.

Inter and intraday analysis of real samples

To evaluate the repeatability and reproducibility of the voltammetric method employing screen-printed electrodes (SPEs), inter- and intra-day precision of three concentrations of the sunitinib drug were tested. The obtained results are presented in Table S1 of the *Supplementary material*. The low RSD and SD values further confirm the repeatability, reproducibility, and precision of the SPEs in the determination of sunitinib. The values for within-day and between-day precision and accuracy were well within the generally accepted criteria for analytical methods.

Comparison with other sensors

A comparison of the SPE electrode performance for STB determination with some previously reported works is shown in Table 2.

As far as we know, this is the third reported electrochemical sensor for the detection of the anticancer drug sunitinib malate. Compared to the previous works on modifications of GCE, our indigenously prepared bare SPE could sense STB from 0.08 to 88 µM with a high sensitivity of 0.386 µA μM^{-1} cm^{-2}. On analysing the oxidation potentials of various electrodes (polyacrylonitrile/ /nanofibers/Ni-Zn- ferrite composite) at 0.66 V [3] and modified GCE at 0.64 V [44], our sensor has

a lower oxidation potential of 0.45 V. The limit of detection for this developed sensor was found to be 0.009 µM (9 nM). The low cost, easy fabrication procedure, and high selectivity make our sensor a good candidate for TDM analysis. Concerning the matrix, the linear range and limit of detection of other chromatographic techniques and the developed method have been evaluated and tabulated in Table 2.

***Table 2**. Comparison of matrix, dynamic range of detection, and LOD for the detection of STB with previously reported chromatographic and electrochemical methods*

Method	Matrix	Linear range, µM	LOD, nM	Ref.
HPLC/MS/MS	Serum	0.003 to 0.94	0.002	[17]
HPLC/UV-Vis	Tablet	0.037 - 0.37	0.02	[43]
UPLC/MS/MS	Serum	0.003 - 0.094	0.002	[44]
Fluorescent/N-GQDs[1]	Serum	0.094-37.55	0.03	[13]
Polyacrylonitrile nanofibers/$Ni_{0.5}Zn_{0.5}Fe_2O_4$ nanoparticles	Serum	0.018-18.77	0.9	[3]
Modified GCE	Plasma	0.1 - 1	0.1	[5]
Metal-organic frameworks and carbon nanotubes nanocomposite	Urine and serum	0.02 - 30	5	[45]
GCE modified with a novel composite of synthesized graphitic carbon nitride (g-C_3N_4) and $CoNiO_2$ bimetallic oxide nanoparticles (g-C_3N_4/$CoNiO_2$)	Urine, serum and capsule	0.1-83.8	52	[46]
Indigenously prepared SPE	Urine, blood and tablets	0.08 - 88	9	This work

[1]N-GQDS = nitrogen doped graphene quantum dots

The currently employed STB detection uses hyphenated approaches (HPLC-UV, HPLC-MS, GC-MS) and chromatography-based methods (GC, HPLC). These methods require sophisticated working procedures, multistage sample preparation, and tedious extraction. Due to its high hydrophilicity, STB and its active metabolites are difficult to separate from biological matrices. Platforms for electrochemical sensors are most suited for quick and accurate STB point-of-care sensing. The quick, accurate, and cost-effective instrumentation makes the electrochemical platforms superior to the existing spectrophotometric and chromatographic methods.

Conclusion

A disposable screen-printed electrode for the selective detection of the anticancer drug sunitinib malate (STB) was successfully developed. The dynamic range of the developed sensor is 0.08 to 88 µM STB in 0.1 M PB with a sensitivity of 0.386 µA μM^{-1} cm^{-2}. Since the expected plasma concentrations of sunitinib are much higher than the sensor's detection range, the sensor can be used for real sample analysis. Hence, our sensor will help in the TDM analysis of the drug sunitinib in samples. Interference studies further confirmed that the sensor has high selectivity towards the STB at an oxidation potential of 0.45 V *vs.* Ag/AgCl. Real sample analysis was performed with blood and urine samples, and the high recovery values obtained show the suitability of sensors for testing drugs from patient samples. The sensor response was found to be highly reproducible, with an RSD value of 3.49 %.

In moving forward, future research directions should focus on enhancing the performance of electrochemical sensors for sunitinib malate detection. This includes exploring miniaturization efforts aiming towards developing portable devices suitable for point-of-care testing while integrating sensor arrays that could enable simultaneous detection of multiple analytes relevant to cancer therapy. By real-time monitoring of drug levels in the bloodstream, these types of sensors enable personalized therapies suited to each patient's specific requirements. This ensures receiving

the best possible dosage of the drug, maximising therapeutic efficacy while minimising negative side effects and toxicity. Because of their high sensitivity and specificity, these sensors can detect drug concentrations early, allowing for appropriate therapeutic modifications. This can help to avoid underdosing, which can lead to unsuccessful treatment, as well as overdose, which can have major repercussions. As a result, patients' treatment is better handled, with fewer adverse effects. Furthermore, the portability and simplicity of electrochemical sensors allow for regular and convenient monitoring away from hospital settings. This lowers the need for frequent hospital visits, improves patients' quality of life, and allows for more flexible and manageable treatment plans. Overall, the incorporation of electrochemical sensors within cancer therapy can result in more accurate and effective treatment approaches, increased patient adherence to drug regimens, and better overall results, making cancer treatment more responsive and patient-focused.

Supplementary material: *Additional data are available electronically on article page of the journal's website: https://pub.iapchem.org/ojs/index.php/JESE/article/view/2478, or from the corresponding author upon request.*

Acknowledgements: *The authors greatly thank Sahrdaya College of Engineering and Technology for the faculty research seed money grant (FRSG) and the research facilities provided to conduct this research study. The authors are thankful to Mr. Arjun Warrier, Research Scholar at Vellore Institute of Technology (VIT), Tamil Nadu, for recording FE-SEM and Mr. A. S. Shanu, Research Scholar at St. Thomas' College (Autonomous), Thrissur, for recording the XRD spectrum. Authors wish to thank the Central Instrumentation Facility, IIT Palakkad, Kerala for providing the facility to perform EIS for the experiment.*

Funding: *The authors report funding from the Kerala Startup Mission for the financial support provided by IDEAFEST 2022 (KSUM/966/2022 dated November 7, 2022). Ms Pooja Das M. express her sincere thanks to APJ Abdul Kalam Kerala Technological University, established by the Government of Kerala, for providing financial assistance in the form of the Centre for Engineering Research and Development (CERD) PhD Fellowship Programme, 2020 (U.O.No. 539/2021/KTU dated 25th March 2021).*

Conflict of interest: *The authors declare that they have no conflict of interest.*

Availability of data: *Data are available on request to the corresponding author.*

Authors' contributions: *A. Warrier and P. Das Manjulabhai performed the measurements and contributed equaly; D. Gangadharan and J. Raveendran were involved in planning and supervised the work, A. Warrier, P. Das Manjulabhai, A. Rajesh., U. Shanmughan and V. Vijayakumar processed the experimental data, performed the analysis, while A. Warrier. and P. Das Manjulabhai. drafted the manuscript, designed the figures, and performed the calculations. D. Gangadharan and J. Raveendran aided in interpreting the results and worked on the manuscript. All authors discussed the results and commented on the manuscript. A.Warrier and P.Das Manjulabhai wrote the paper with input from all authors.*

Ethics approval: *Not applicable*

References

[1] K. Patel, S. Siraj, C. Smith, M. Nair, J. K. Vishwanatha, R. Basha, Pancreatic cancer: an emphasis on current perspectives in immunotherapy, *Critical Reviews in Oncogenesis* **24** (2019) 105-118. https://doi.org/10.1615/critrevoncog.2019031417

[2] T. Sinha, Tumors: benign and malignant, *Cancer Therapy & Oncology International Journal* **10** (2018) 52-54. https://doi.org/10.19080/CTOIJ.2018.10.555790
[3] A. Yarahmadi, T. Madrakian, A. Afkhami, N. R. Jalal, Electrochemical determination of sunitinib in biological samples using polyacrylonitrile nanofibers/nickel-zinc-ferrite nanocomposite/carbon paste electrode, *Journal of The Electrochemical Society* **166** (2019) B1268. https://doi.org/10.1149/2.0371914jes
[4] Y.-L. Lai, C.-C. Lin, S.-R. Hsu, S.-K. Yen, Electrochemical deposition of cisplatin on pure magnesium, *Journal of The Electrochemical Society* **165** (2018) D196. https://doi.org/10.1149/2.0501805JES/XML
[5] L. Cabel, B. Blanchet, A. Thomas-Schoemann, O. Huillard, A. Bellesoeur, A. Cessot, J. Giroux, P. Boudou-Rouquette, R. Coriat, M. Vidal, N. E. B. Saidu, L. Golmard, J. Alexandre, F. Goldwasser, Drug monitoring of sunitinib in patients with advanced solid tumors: a monocentric observational French study, *Fundamental and Clinical Pharmacology* **32** (2018) 98-107. https://doi.org/10.1111/fcp.12327
[6] N. P. Van Erp, S. D. Baker, A. S. Zandvliet, B. A. Ploeger, M. Den Hollander, Z. Chen, J. Den Hartigh, J. M. C. König-Quartel, H.-J. Guchelaar, H. Gelderblom, Marginal increase of sunitinib exposure by grapefruit juice, *Cancer Chemotherapy and Pharmacology* **67** (2011) 695-703. https://doi.org/10.1007/s00280-010-1367-0
[7] G. D. Demetri, A. T. van Oosterom, C. R. Garrett, M. E. Blackstein, M. H. Shah, J. Verweij, G. McArthur, I. R. Judson, M. C. Heinrich, J. A. Morgan, J. Desai, C. D. Fletcher, S. George, C. L. Bello, X. Huang, C. M. Baum, P. G. Casali, Efficacy and safety of sunitinib in patients with advanced gastrointestinal stromal tumour after failure of imatinib: a randomised controlled trial, *The Lancet* **368** (2006) 1329-1338. https://doi.org/10.1016/S0140-6736(06)69446-4
[8] S. M. Tange, V. L. Grey, P. E. Senécal, Therapeutic drug monitoring in pediatrics: a need for improvement, *The Journal of Clinical Pharmacology* **34** (1994) 200-214. https://doi.org/10.1002/J.1552-4604.1994.TB03987.X
[9] A. M. AboulMagd, N. S. Abdelwahab, Analysis of sunitinib malate, a multi-targeted tyrosine kinase inhibitor: A critical review, *Microchemical Journal* **163** (2021) 105926. https://doi.org/10.1016/J.MICROC.2021.105926
[10] E. Souri, E. Amoon, N. S. Ravari, F. Keyghobadi, M. B. Tehrani, Spectrophotometric methods for determination of sunitinib in pharmaceutical dosage forms based on ion-pair complex formation, *Iranian Journal of Pharmaceutical Research* **19** (2020) 103. https://doi.org/10.1016/10.22037/ijpr
[11] R. Demlová, M. Turjap, O. Peš, K. Kostolanská, J. Juřica, Therapeutic drug monitoring of sunitinib in gastrointestinal stromal tumors and metastatic renal cell carcinoma in adults—a review, *Therapeutic Drug Monitoring* **42** (2020) 20-32. https://doi.org/10.1097/FTD.0000000000000663
[12] R. M. Silva, A. D. da Silva, J. R. Camargo, B. S. de Castro, L. M. Meireles, P. S. Silva, B. C. Janegitz, T.A. Silva, Carbon nanomaterials-based screen-printed electrodes for sensing applications, *Biosensors (Basel)* **13** (2023) 453. https://doi.org/10.3390/bios13040453
[13] H. M. Kashani, T. Madrakian, A. Afkhami, Highly fluorescent nitrogen-doped graphene quantum dots as a green, economical and facile sensor for the determination of sunitinib in real samples, *New Journal of Chemistry* **41** (2017) 6875-6882. https://doi.org/10.1039/C7NJ00262A
[14] B. Vercelli, S. Crotti, M. Agostini, Voltammetric responses at modified electrodes and aggregation effects of two anticancer molecules: irinotecan and sunitinib, *New Journal of Chemistry* **44** (2020) 18233-18241. https://doi.org/10.1039/D0NJ03896B

[15] J. Ye, M. Bi, H. Yao, D. Yang, D. Chen, Chromatographic and mass spectrometric analytical strategies for profiling tyrosine kinase inhibitors in biological samples, *Microchemical Journal* **201** (2024) 110694. http://dx.doi.org/10.1016/j.microc.2024.110694

[16] G. Zotti, A. Berlin, B. Vercelli, Electrochemistry of conjugated planar anticancer molecules: Irinotecan and Sunitinib, *Electrochimica Acta* **231** (2017) 336-343. http://dx.doi.org/10.1016/j.electacta.2017.02.043

[17] P. Minkin, M. Zhao, Z. Chen, J. Ouwerkerk, H. Gelderblom, S. D. Baker, Quantification of sunitinib in human plasma by high-performance liquid chromatography-tandem mass spectrometry, *Journal of Chromatography B* **874** (2008) 84-88. https://doi.org/10.1016/j.jchromb.2008.09.007

[18] L. Litti, V. Amendola, G. Toffoli, M. Meneghetti, Detection of low-quantity anticancer drugs by surface-enhanced Raman scattering, *Analytical and Bioanalytical Chemistry* **408** (2016) 2123-2131. https://doi.org/10.1007/s00216-016-9315-4

[19] M. Rodamer, P. W. Elsinghorst, M. Kinzig, M. Gütschow, F. Sörgel, Development and validation of a liquid chromatography/tandem mass spectrometry procedure for the quantification of sunitinib (SU11248) and its active metabolite, N-desethyl sunitinib (SU12662), in human plasma: application to an explorative study, *Journal of Chromatography B* **879** (2011) 695-706. https://doi.org/10.1016/j.jchromb.2011.02.006

[20] C. Zhang, L. Li, Study on electrochemical sensor for sunitinib cancer medicine based on metal-organic frameworks and carbon nanotubes nanocomposite, *Alexandria Engineering Journal* **97** (2024) 8-13. https://doi.org/10.1016/j.aej.2024.03.104

[21] F. Y. Dewi, S. T. Cahyono, F. Hilmi, A. R. Sanjaya, D. W. Hastuti, N. I. Pratiwi, H. K. Aliwarga, P. Prajitno, T.A. Ivandini, D. Handoko, *Electrochemical performance of gold nanoparticles decorated on Multi-walled Carbon Nanotube (MWCNT) Screen-printed Electrode (SPE)*, in: ITM Web of Conferences, 2024, p. 1019. https://doi.org/10.1051/itmconf/20246101019

[22] A. L. Devi, P. E. Resmi, A. Pradeep, P. V Suneesh, B. G. Nair, T. G. S. Babu, A paper-based point-of-care testing device for the colourimetric estimation of bilirubin in blood sample, *Spectrochimica Acta Part A: Molecular and Biomolecular Spectroscopy* **287** (2023) 122045. https://doi.org/10.1016/J.MATLET.2021.130574.

[23] M. H. Ali, M. A. K. Azad, K. A. Khan, M. O. Rahman, U. Chakma, A. Kumer, Analysis of crystallographic structures and properties of silver nanoparticles synthesized using PKL extract and nanoscale characterization techniques, *ACS Omega* **8** (2023) 28133-28142. https://doi.org/10.1021/acsomega.3c01261

[24] Y. Wang, J. E. Panzik, B. Kiefer, K. K. M. Lee, Crystal structure of graphite under room-temperature compression and decompression, *Scientific Reports* **2** (2012) 520. https://doi.org/10.1038/srep00520

[25] M. A. Majeed Khan, S. Kumar, M. Ahamed, S. A. Alrokayan, M. S. AlSalhi, Structural and thermal studies of silver nanoparticles and electrical transport study of their thin films, *Nanoscale Research Letters* **6** (2011) 434. https://doi.org/10.1186/1556-276X-6-434

[26] M. BinSabt, M. Shaban, A. Gamal, Nanocomposite electrode of titanium dioxide nanoribbons and multiwalled carbon nanotubes for energy storage, *Materials* **16** (2023) 595. https://doi.org/10.3390/ma16020595

[27] F. S. da Cruz, F. de Souza Paula, D. L. Franco, W. T. P. dos Santos, L. F. Ferreira, Electrochemical detection of uric acid using graphite screen-printed electrodes modified with Prussian blue/poly (4-aminosalicylic acid)/Uricase, *Journal of Electroanalytical Chemistry*. **806** (2017) 172-179. http://dx.doi.org/10.1016/j.jelechem.2017.10.070

[28] K. Jyoti, M. Baunthiyal, A. Singh, Characterization of silver nanoparticles synthesized using Urtica dioica Linn. leaves and their synergistic effects with antibiotics, *Journal of Radiation Research and Applied Sciences* **9** (2016) 217-227. https://doi.org/10.1016/j.jrras.2015.10.002

[29] H. Pal, V. Sharma, R. Kumar, N. Thakur, Facile synthesis and electrical conductivity of carbon nanotube reinforced nanosilver composite, *Zeitschrift für Naturforschung A* **67a** (2012) 679-684. https://doi.org/10.5560/zna.2012-0072

[30] M. M. Ngoma, M. Mathaba, K. Moothi, Effect of carbon nanotubes loading and pressure on the performance of a polyethersulfone (PES)/carbon nanotubes (CNT) membrane, *Scientific Reports* **11** (2021) 23805. https://doi.org/10.1038/s41598-021-03042-z

[31] H. Rahmanian, Z. Es'haghi, M. Dadmehr, A robust electrochemical sensing platform for the detection of erlotinib based on nitrogen-doped graphene quantum dots/copper nanoparticles-polyaniline-graphene oxide nanohybrid, *Nanotechnology* **34** (2022) 15502. https://doi.org/10.1088/1361-6528/ac8996

[32] E. C. Okpara, S. C. Nde, O. E. Fayemi, E. E. Ebenso, Electrochemical characterization and detection of lead in water using SPCE modified with BiONPs/PANI, *Nanomaterials* **11** (2021) 1294. https://doi.org/10.3390/nano11051294

[33] N. Negash, H. Alemu, M. Tessema, Electrochemical Characterization and Determination of Phenol and Chlorophenols by Voltammetry at Single Wall Carbon Nanotube/Poly (3, 4-ethylenedioxythiophene) Modified Screen Printed Carbon Electrode, *International Scholarly Research Notices* **2015** (2015) 459246. http://dx.doi.org/10.1155/2015/459246

[34] J. E. B. Randles, Kinetics of rapid electrode reactions, *Discussions of the Faraday Society* **1** (1947) 11-19. https://doi.org/10.1039/DF9470100011

[35] J. Raveendran, J. Stanley, T. G. S. Babu, Voltammetric determination of bilirubin on disposable screen printed carbon electrode, *Journal of Electroanalytical Chemistry*. **818** (2018) 124-130. https://doi.org/10.1016/J.JELECHEM.2018.04.020

[36] A.J. Bard, L.R. Faulkner, *Electrochemical methods: fundamentals and applications*, Wiley, New-York, 1989. ISBN 0-471-05542-5

[37] A. Bruchbacher, S. Nachbargauer, H. Fajkovic, M. Schmidinger, Sunitinib Dose Escalation in Metastatic Renal Cell Carcinoma, *Kidney Cancer* **3** (2019) 103-110. https://doi.org/10.3233/KCA-190055

[38] N. A. G. Lankheet, I. M. E. Desar, S. F. Mulder, D. M. Burger, D. M. Kweekel, C. M. L. van Herpen, W.T.A. van der Graaf, N.P. van Erp, Optimizing the dose in cancer patients treated with imatinib, sunitinib and pazopanib, *British Journal of Clinical Pharmacology* **83** (2017) 2195-2204. https://doi.org/10.1111/bcp.13327

[39] S. Huang, X. Liu, X. Guo, H. Wu, H. Lu, Z. Pan, S. Cai, X. Wu, X. Zhang, Sunitinib versus imatinib dose escalation after failure of imatinib standard dose in patients with advanced Gastrointestinal stromal tumors-a real-world multi-center study, *Translational Oncology* **30** (2023) 101641. https://doi.org/10.1016/j.tranon.2023.101641

[40] C. Serrano, A. Mariño-Enríquez, D. L. Tao, J. Ketzer, G. Eilers, M. Zhu, C. Yu, A. M. Mannan, B. P. Rubin, G. D. Demetri, others, Complementary activity of tyrosine kinase inhibitors against secondary kit mutations in imatinib-resistant gastrointestinal stromal tumours, *British Journal of Cancer* **120** (2019) 612-620. https://doi.org/10.1038/s41416-019-0389-6

[41] E. Wang, S. G. DuBois, C. Wetmore, A. C. Verschuur, R. Khosravan, Population pharmacokinetics of sunitinib and its active metabolite SU012662 in pediatric patients with gastrointestinal stromal tumors or other solid tumors, *European Journal of Drug Metabolism and Pharmacokinetics* **46** (2021) 343-352. https://doi.org/10.1007/s13318-021-00671-7

[42] F. Budak, A. Cetinkaya, S. I. Kaya, E. B. Atici, S. A. Ozkan, Investigations on the electrochemical behavior of sunitinib and metabolites N-desethyl-sunitinib and sunitinib-N-oxide and its selective determination using molecularly imprinted polymer-based sensor, *Electrochimica Acta* **472** (2023) 143434. http://dx.doi.org/10.1016/j.electacta.2023.143434

[43] B. Blanchet, C. Saboureau, A. S. Benichou, B. Billemont, F. Taieb, S. Ropert, A. Dauphin, F. Goldwasser, M. Tod, Development and validation of an HPLC-UV-visible method for sunitinib

quantification in human plasma, *Clinica Chimica Acta* **404** (2009) 134-139. https://doi.org/10.1016/j.cca.2009.03.042

[44] P. de Bruijn, S. Sleijfer, M.-H. Lam, R. H. J. Mathijssen, E. A. C. Wiemer, W. J. Loos, Bioanalytical method for the quantification of sunitinib and its n-desethyl metabolite SU12662 in human plasma by ultra performance liquid chromatography/tandem triple-quadrupole mass spectrometry, *Journal of Pharmaceutical and Biomedical Analysis.* **51** (2010) 934-941. https://doi.org/10.1016/j.jpba.2009.10.020

[45] C. Zhang, L. Li, Study on electrochemical sensor for sunitinib cancer medicine based on metal-organic frameworks and carbon nanotubes nanocomposite, *Alexandria Engineering Journal* **97** (2024) 8-13. https://doi.org/10.1016/j.aej.2024.03.104

[46] G. Kholafazadehastamal, N. Erk, A. A. Genc, Z. Erbas, M. Soylak, Glassy carbon electrodes modified with graphitic carbon nitride nanosheets and $CoNiO_2$ bimetallic oxide nanoparticles as electrochemical sensor for Sunitinib detection in human fluid matrices and pharmaceutical samples, *Microchimica Acta* **191** (2024) 527. https://doi.org/10.1007/s00604-024-06605-9